MCB
Journals.ASM.org

Multiple Cancer Testis Antigens Function To Support Tumor Cell Mitotic Fidelity

Kathryn M. Cappell, Rebecca Sinnott, Patrick Taus, Kimberly Maxfield, Moriah Scarbrough, and Angelique W. Whitehurst

Department of Pharmacology and Lineberger Comprehensive Cancer Center, University of North Carolina at Chapel Hill, Chapel Hill, North Carolina, USA

While the expression of genes that are normally involved in spermatogenesis is frequently detected in tumors, the extent to which these gene products are required for neoplastic behaviors is unclear. To begin to address their functional relevance to tumorigenesis, we identified a cohort of proteins which display synthetic lethality with paclitaxel in non-small-cell lung cancer and whose expression is biased toward testes and tumors. Remarkably, these testis proteins, FMR1NB, NXF2, MAGEA5, FSIP1, and STARD6, are required for accurate chromosome segregation in tumor cells. Their individual depletion enhances the generation of multipolar spindles, increases mitotic transit time, and induces micronucleation in response to an otherwise innocuous dose of paclitaxel. The underlying basis for abnormal mitosis is an alteration in microtubule function, as their depletion increases microtubule cytaster formation and disrupts microtubule stability. Given these observations, we hypothesize that reactivated testis proteins may represent unique tumor cell vulnerabilities which, if targeted, could enhance responsiveness to antimitotic therapy. Indeed, we demonstrate that combining paclitaxel with a small-molecule inhibitor of the gametogenic and tumor cell mitotic protein TACC3 leads to enhanced centrosomal abnormalities, activation of death programs, and loss of anchorage-independent growth.

Tumor-specific epigenetic alterations allow the activation of a panoply of otherwise silenced genetic programs that can be exploited to promote neoplastic phenotypes. In particular, genes normally involved in development and gametogenesis are frequently found to be reactivated in tumors, affording an opportunity for transformed cells to co-opt primordial cell features to confer oncogenic behaviors such as self-renewal, uncontrolled proliferation, and epithelial-to-mesenchymal transition (EMT) (1, 39). Cancer testis (CT) antigens represent one group of gametogenic proteins whose expression is otherwise biased toward the testes and reactivated in tumor cells (39). Because the testes are an immune privileged site, humoral and/or cellular responses are often elicited to CT antigens in cancer patients. Thus, much focus has surrounded exploiting these antigens as anticancer vaccine targets, while functional roles, if any, for these proteins in supporting tumor cell fitness have not been extensively evaluated. There are over 200 annotated CT antigens, and most have no known role in spermatogenesis or tumorigenesis (39). However, three recent studies implicate members of the CT antigen family in tumorigenic processes, including p53 turnover, centrosome coalescence, mitotic progression, and regulation of retinoic acid signaling (10, 12, 43). Furthermore, high expression of specific CT antigens in tumors has been correlated with significantly poorer outcomes, suggesting that their reactivation may enhance aggressiveness or chemoresistance (8, 12, 43). Therefore, uncovering roles for CT antigens and other ectopically expressed gametogenic genes could significantly enhance our understanding of how tumor cells engage otherwise anomalous components to support proproliferative activities.

Employing a pangenomic loss-of-function strategy, we previously found that the CT antigen acrosin binding protein (ACRBP) supports mitotic spindle fidelity in tumor cells by regulating NUMA1 protein levels and thereby reinforces bipolar spindle assembly in the presence of paclitaxel (42, 43). These observations suggest that one role for reactivated spermatogenic proteins is to buttress mitotic progression, making tumor cells less susceptible to mitotic perturbations. To develop this hypothesis further, we asked whether this role was unique to ACRBP or if other CT antigens also functioned to support mitotic progression. To examine this, we mined a genome-wide small interfering RNA (siRNA) data set for paclitaxel sensitizer genes that either were classified as CT antigens or were reported to have a testis-biased expression pattern. We then assessed the contribution of genes meeting this criterion to chromosome segregation, bipolar spindle formation, and interphase microtubule dynamics. Here, we report a novel role for 5 of these testis proteins, FMR1NB, NXF2, MAGEA5, FSIP1, and STARD6, in supporting mitosis in NSCLC cells. These findings suggest that anomalously expressed gene products may reinforce mitotic progression and thus diminish the negative impacts of spindle poisons, such as paclitaxel. Direct targeting of this molecular buffer may enhance the effectiveness of first-line therapeutics. In support of this hypothesis, we pharmacologically validated the enhanced tumoricidal activity of combining paclitaxel with a small-molecule inhibitor of one of these testis proteins, TACC3, a well-established component of the mitotic machinery in tumor cells. These findings may reflect a paradigm in which reactivated gametogenic programs can be engaged by tumor cells to buttress essential processes that support tumor fecundity.

MATERIALS AND METHODS

Cell culture. NSCLC cell lines were maintained in RPMI medium (Gibco) with 5% fetal bovine serum (FBS). HBEC30 and HCC4017 cell lines were maintained in ACL-4 medium (14a) plus 2% FBS. The HBEC3 isogenic series was a gift from John Minna and has been described previously (31, 34). These cells were maintained in keratinocyte medium supplemented with supplied epidermal growth factor and bovine pituitary extract

Received 1 June 2012 Returned for modification 10 July 2012
Accepted 1 August 2012
Published ahead of print 6 August 2012
Address correspondence to Angelique W. Whitehurst, awhit1@med.unc.edu.
Supplemental material for this article may be found at http://mcb.asm.org/.

doi:10.1128/MCB.00686-12

TABLE 1 Testis or placental genes identified as chemosensitizers from a genome-wide siRNA paclitaxel synthetic lethal screen

Gene	Expression pattern	CT antigen[a]	Name	Function in the testes/developing gamete
ACRBP	Testis enriched (39)	Y	Acrosin binding protein	Binds acrosin in spermatids
FMR1NB	Testis enriched (39)	Y	Fragile X mental retardation neighbor 1	Unknown
NXF2	Testis enriched (39)	Y	Nuclear RNA export factor 2	mRNA export into the cytoplasm
MAGEA5	Testis enriched (39)	Y	Melanoma antigen family A, 5	Unknown
STARD6	Testis enriched (4)	N	StAR-related lipid transfer (START) domain containing 6	Mitochondrial sterol transport
TACC3	Bone marrow and testes (2)	N	Transforming, acidic coiled-coil containing protein 3	Mitotic spindle formation in embryogenesis
FSIP1	Germ cell, testes (5)	N	Fibrous sheath interacting protein 1	Component of the sperm flagellum

[a] Y, yes; N, no.

(Gibco). WHIM12 triple-negative breast cancer cells were a kind gift from Matthew Ellis (Washington University, St. Louis, MO). LCOV2 cells were obtained as previously described (43). Paclitaxel (Sigma, Tocris) was resuspended in dimethyl sulfoxide (DMSO). Paclitaxel concentrations used for each cell line were as follows: 10 nM for H1155, HCC366, and H2126; 1.0 nM for HCC515, A549, HCC1993, SUM149, and WHIM12; and 0.1 nM for H460, HCC4017, and HCC15. The identity of all cell lines was validated by short tandem repeat (STR) analysis at multiple points during the study. KHS101 was a kind gift from Peter Schultz (44). Additional KHS101 was synthesized by the UNC Center for Integrative Chemical Biology and Drug Discovery.

siRNA transfections. Transfection conditions were as described previously (42); 50 nM siGENOME Smart pools (ThermoFisher) and appropriate Dharmafect or RNAiMAX transfection reagent were used. As a control, we used either a nontargeting siRNA pool or an siRNA pool targeting DLNB14, for which we have not detected any phenotype upon depletion. For deconvolutions, individual siRNAs were used at a final concentration of 75 to 100 nM (42). For TACC3, an independent pool of siRNAs (ON-TARGETplus) was used for deconvolution at 50 nM.

DNA transfection. cDNAs for myc-tagged genes were reverse transfected into H1299 cells using Lipofectamine 2000. Forty-eight hours posttransfection, cells were fixed for further analysis.

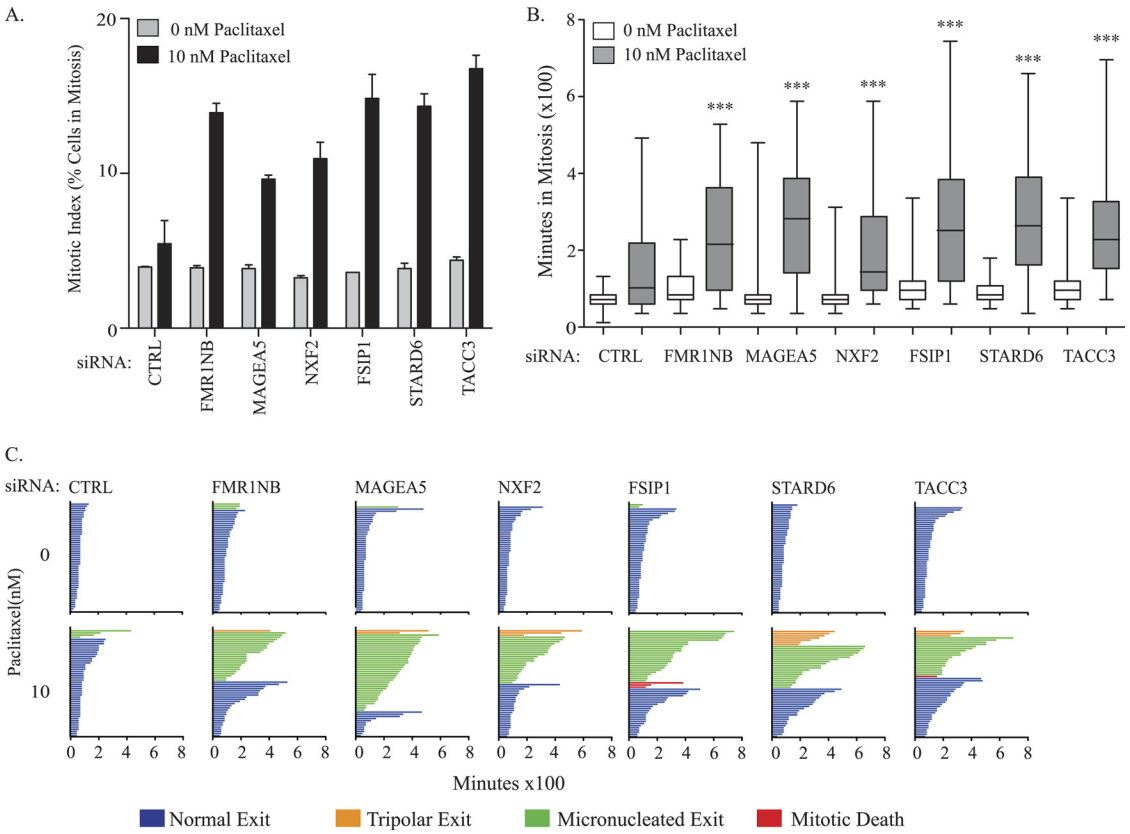

FIG 1 Testis proteins support mitotic spindle fidelity. (A) H1155 cells were transfected with the indicated siRNAs and exposed to 10 nM paclitaxel for 24 h in a 96-well format. Cells were stained with anti-phospho-histone 3B (pH3B), and automated counting using a ThermoFisher ArrayScan quantitated the percentage of cells in mitosis. Error bars represent ranges from the means of 2 independent experiments. (B) H1155 cells stably expressing H2B-GFP were transfected with the indicated siRNAs. Forty-eight hours posttransfection, cells were exposed to paclitaxel or carrier and imaged by time-lapse microscopy for 48 h. Single-cell lineage tracing for each condition was performed to measure the length of mitosis as a function of the time from prometaphase to telophase in 50 cells. Quartile ranges for conditions are shown. *P* values for differences in timing between the control and target transfected at 10 nM were calculated by Mann-Whitney *U* test. ***, $P < 0.001$. (C) Representative examples of time-lapse sequences illustrating heterogeneity of fates exhibited by H1155 cells following depletion of indicated gene products and exposure to a vehicle or 10 nM paclitaxel.

shRNA transductions. Lentivirus was produced per Open Biosystems protocol using short hairpin RNA (shRNA) clones in the PLKO.1 vector from the RNA Consortium. Two hairpins were used per gene, and each was validated for transcript knockdown.

High-content live-cell imaging. Cell lines expressing histone 2B-green fluorescent protein (GFP) (H2B-GFP) were generated by viral transduction as described previously (7). A stable population of H2B-GFP-expressing cells was obtained through fluorescence-activated cell sorting (FACS). The stably expressing cell lines were then treated as described in the figure legends and imaged on a BD Pathway 855 imager using a 20× high-numerical-aperture objective. Images were taken approximately every 15 min for the indicated time periods, and movies were generated using ImageJ.

Quantitative RT-PCR. For confirmation of gene knockdown, RNA was harvested from cells transfected with siRNA for 72 h using the GenElute Mammalian Total RNA Miniprep kit (Sigma). cDNA was generated using 2 to 4 μg of total RNA and the High-Capacity cDNA reverse transcription kit (Applied Biosystems). Real-time PCR (RT-PCR) detection used inventoried TaqMan gene expression assays purchased from Applied Biosystems that are designed to exclusively detect mRNA. Amplification was performed on the 7500 Fast Real Time PCR machine (Applied Biosystems). The ribosomal subunit RPL27 was used as the endogenous control, and differences in expression were calculated using the $2^{-\Delta\Delta CT}$ method. For evaluation of gene expression in various human tissues, total human RNA samples pooled from multiple individuals were obtained from Clontech.

Immunoblotting. Cells were lysed in boiling sample buffer as described previously (7). The primary antibodies used were from Santa Cruz (glyceraldehyde-3-phosphate dehydrogenase [GAPDH] and TACC3). Cleaved caspase-3 antibodies were obtained from Epitomics. Secondary antibodies were horseradish peroxidase-conjugated anti-mouse and anti-rabbit IgG (Jackson ImmunoResearch).

Immunofluorescence. Conditions for immunofluorescence were as described previously (7). Briefly, cells were grown on glass coverslips and fixed at various time points in 3.7% formaldehyde or MeOH, specifically for γ-tubulin staining. Primary antibodies used were anti-β-tubulin (Sigma) and antipericentrin (Abcam). Secondary antibodies were Alexa Fluor-conjugated anti-mouse or anti-rabbit antibodies (Invitrogen). Images were acquired using a Zeiss Axiovision upright fluorescence microscope with either a 10×, 20×, or 40× objective. All images taken to compare samples used identical gain and exposure settings.

Soft agar assay. H1155 cells (1×10^4 to 1×10^6) were resuspended in 0.5% Bacto agar in complete medium and overlaid on solidified 0.5% Bacto agar in 60-mm dishes. After solidification, a top layer of complete medium was added. For drug treatments, half the medium from the top layer was removed and replaced with medium containing 2× the final drug concentration and 2× fetal bovine serum. Colonies were grown for 2 weeks and then stained with 0.005% crystal violet in phosphate-buffered saline (PBS) overnight.

Microtubule regrowth assay. Cells grown on glass coverslips were depolymerized with 11 μM nocodazole (Calbiochem) for 30 min. After depolymerization, cells were washed and allowed to recover in warm medium. Depolymerized microtubules were extracted in 0.2% Triton X-100 in PHEM buffer (60 mM PIPES [pH 7.0], 25 mM HEPES, 100 mM EGTA, 2 mM $MgCl_2$, 1 μM paclitaxel), and slips were then fixed in 3.7% formaldehyde. The microtubule network was stained with β-tubulin (Sigma), γ-tubulin (Sigma), and pericentrin (Abcam). All images for comparison among samples were acquired using identical exposure and gain settings using the Zeiss AxioVision software package. For quantitation, individual cells were circled based on their fluorescent signals. ImageJ calculated the area and integrated mean intensity. The corrected total cell fluorescence (CTCF) was calculated as integrated density − (area of selected cell × mean fluorescence of background reading). At least 50 cells were analyzed over two experiments.

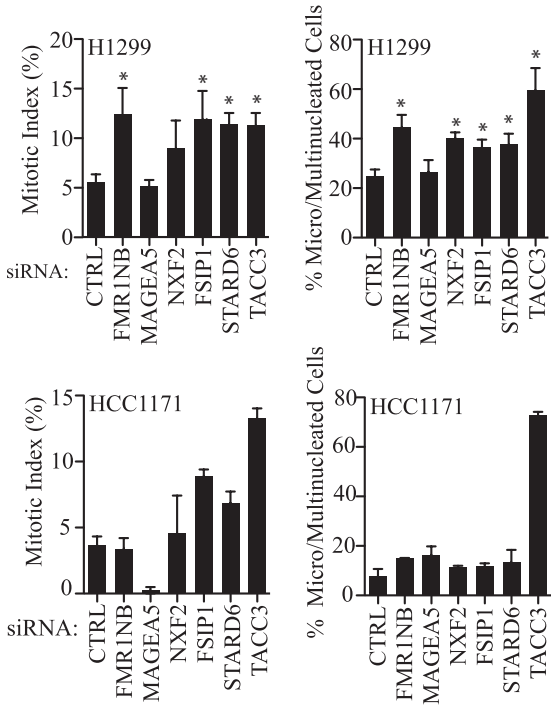

FIG 2 Depletion of sperm proteins induces mitotic arrest or defects in H1299 and HCC1171 cells. Cells were transfected with the indicated siRNAs for 48 h, followed by exposure to 1 nM paclitaxel for 24 h. Cells were immunostained with antibodies recognizing pH3B and antitubulin. DNA was stained with 4′,6-diamidino-2-phenylindole (DAPI). The percentage of cells in mitosis or micro- or multinucleated was manually quantitated. H1299 error bars represent SEMs from 3 independent experiments. *, $P < 0.05$ by Student's *t* test. HCC1171 error bars represent average deviations from the means of 2 independent experiments. At least 150 cells were counted per condition in each experiment.

RESULTS

A cohort of gametogenic proteins is required for accurate chromosome segregation following exposure to low-dose paclitaxel. We have previously employed a pangenomic loss-of-function approach to identify components that modulate responsiveness in NSCLC cells. This strategy revealed that the CT antigen ACRBP can contribute to mitotic fidelity and paclitaxel sensitivity, suggesting that reactivated testis genes may become tumor cell-selective dependencies for cell division. To determine if additional CT antigens or testis genes modulate paclitaxel sensitivity, we combined those genes in the lowest 2.5% rank of paclitaxel sensitizer ratios with a false-discovery rate of <10% as well as all genes scoring 2.5 standard deviations below the mean. This data set contained 409 candidate paclitaxel sensitizers among which we identified 4 CT antigens (ACRBP, FMR1NB, MAGEA5, and NXF2) as well as 3 genes with a testis-biased expression pattern and a documented role in supporting spermatogenesis (FSIP1, STARD6, and TACC3) (Table 1) (2, 4, 5, 11, 39). We validated that mRNA encoded by these genes was expressed in the NSCLC cells employed in the original screen, H1155 (see Fig. S1A in the supplemental material). In addition, we validated that the mRNA expression level of these genes was biased to the testes (see Fig. S1B in the supplemental material). With respect to spermatogenesis, NXF2, FSIP1, and STARD6 have been implicated in mRNA transport/meiosis, fibrous sheath function,

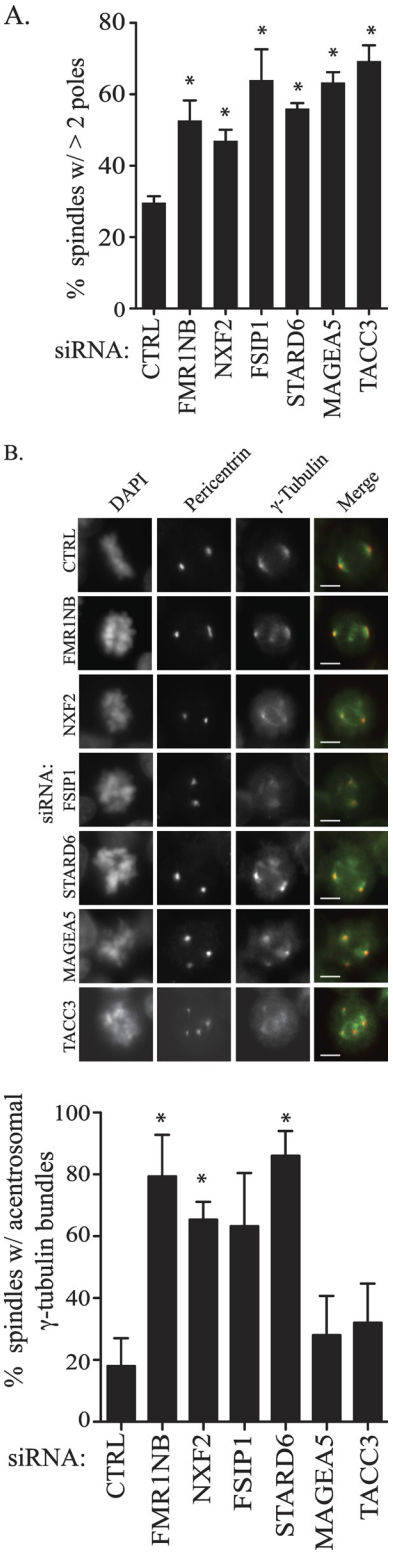

FIG 3 Depletion of CT antigens enhances spindle multipolarity and γ-tubulin bundles. (A) H1155 cells were transfected with the indicated siRNAs. Forty-eight hours posttransfection, cells were exposed to either a vehicle or 10 nM paclitaxel for 24 h. Cell were fixed and immunostained with antibodies specific for γ-tubulin (green) and pericentrin (red) as well as DAPI to visualize DNA. Abnormal mitotics were scored as cells having >2 spindle poles marked by either pericentrin or γ-tubulin foci. The average of 3 experiments is graphed. Error bars represent SEMs. *, *P* value < 0.02 by Student's *t* test compared to the control. (B) Representative epifluorescence images of H1155 cells counted in panel A (top) and quantitation of colocalization of γ-tubulin and pericentrin (bottom). The average of 3 experiments is graphed. Error bars represent SEMs. *, *P* value < 0.02 by Student's *t* test compared to the control. Scale bars represent 5 μm.

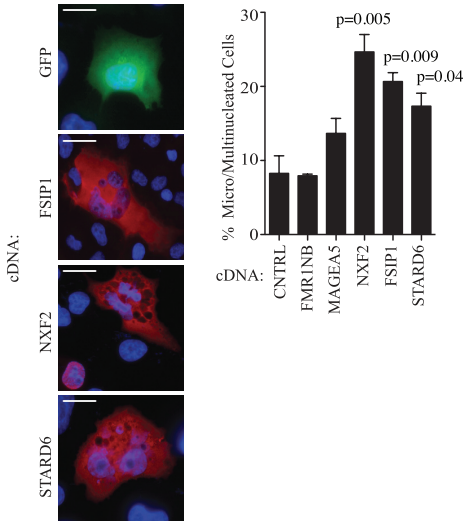

FIG 4 FSIP1, STARD6, and NXF2 overexpression enhance chromosome segregation defects. cDNAs encoding indicated myc-tagged proteins were transfected into H1299 cells. Forty-eight hours posttransfection, cells were fixed and immunostained with anti-myc (red) and anti-β-tubulin (green) antibodies and DAPI. (Left) Representative images of GFP or anti-myc and DAPI stain. Scale bars represent 10 μm. (Right) Multinucleated cells were scored microscopically and are graphed as the fraction of total transfected cells. Error bars represent SEMs from 3 independent experiments. *P* values were calculated with Student's *t* test.

and cholesterol transport, respectively (4, 5, 20, 29, 41). A role for FMR1NB in spermatogenesis has not been reported. TACC3, which is reactivated in a wide range of tumor types, is the best-characterized member of this cohort, with a demonstrated role in embryonic development and differentiation. However, with the exception of TACC3 and ACRBP, no tumorigenic role has been identified for these testis genes (2, 9, 15, 19, 33, 35–37).

Given the phenotypic collaboration observed with the mitotic spindle poison paclitaxel, we first sought to determine if individual depletion of members of this cohort (FMR1NB, MAGEA5, NXF2, FSIP1, STARD6, and TACC3) leads to chromosome segregation defects in the presence of low-dose paclitaxel. We quantitated the mitotic index, a measure of potential mitotic error and arrest, in H1155 NSCLC cells depleted of each testis protein in the presence and absence of paclitaxel. Disruption of candidates alone did not significantly impact the accumulation of mitotic figures. However, exposure of target-depleted cells to 10 nM paclitaxel increased the frequency of mitotic figures relative to controls, potentially indicating a mitotic arrest (Fig. 1A). To determine if the enhanced mitotic index reflected an increase in length of mitosis, we employed live-cell imaging to monitor chromatin dynamics in real time using H1155 cells stably expressing H2B-GFP. Again, depletion of individual testis proteins alone did not alter mitotic transit time compared to the control. However, target-depleted cells exposed to 10 nM paclitaxel were delayed in mitosis signifi-

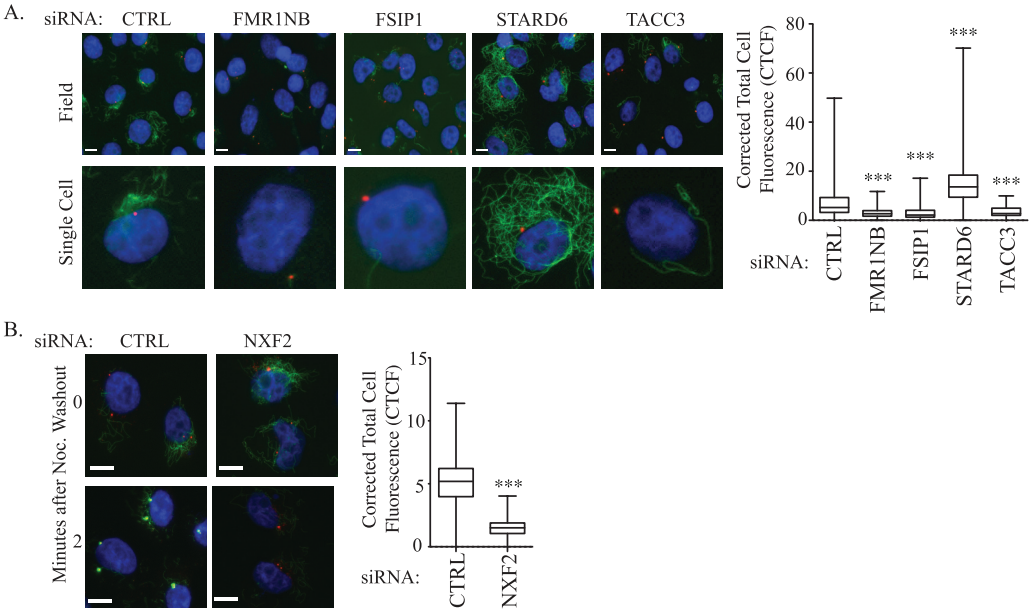

FIG 5 Microtubule function is altered in tumor cells and supported by CT antigens. (A) H1299 cells were transfected with the indicated siRNAs. Seventy-two hours posttransfection, cells were treated with nocodazole for 30 min, fixed, and stained with DAPI (blue), tubulin (green), and pericentrin (red). (Left) Representative images of immunostained cells; (right) quantitation of fluorescence of immunostained cells. (B) Cells were treated as described for panel A, but cells were washed of nocodazole and placed in growth medium for 2 min before fixation. Scale bars are 10 μm.

cantly longer than the control (Fig. 1B). This increase in timing was due to an inability of chromosomes to properly align on the metaphase plate and was aberrantly resolved by mitotic slippage that led to either micronucleation or nuclear fragmentation and/or division into more than 2 daughter cells (Fig. 1C). Thus, these proteins may contribute to chromosome alignment, and their depletion weakens this process sufficiently to increase the sensitivity of cells to mitotic perturbagens. Indeed, a similar stress-induced phenotype is observed following disruption of TACC3, a well-documented component of the mitotic spindle (Fig. 1). Similarly, MAD2 knockout flies display a normal mitosis unless exposed to an antimitotic (6). At least two individual siRNAs within each pool, or an independent pool, recapitulated either a mitotic or apoptotic phenotype for each gene tested (see Fig. S2 in the supplemental material).

To evaluate the functional penetrance of each member of the testis cohort in additional genetic backgrounds, we examined mitotic defects following depletion of each protein together with exposure to paclitaxel in two additional NSCLC cell lines: H1299 and HCC1171 (Fig. 2). FSIP1 and STARD6 depletion enhanced paclitaxel-induced mitotic arrest and/or the formation of micronucleated cells in both lines. FMR1NB and NXF2 depletion had observable consequences on mitosis in H1299 cells but not HCC1171 cells. Mitotic defects were not observed following depletion of MAGEA5 in either H1299 or HCC1171 cells. As expected, TACC3 depletion enhanced paclitaxel-induced mitotic defects in both H1299 and HCC1171 cells. These defects are similar to the enhanced mitotic timing and missegregation of chromosomes we observed by live-cell imaging in H1155 cells (Fig. 1B and C). Thus, the requirement for these testis proteins in supporting accurate chromosome segregation during paclitaxel exposure is a general phenomenon employed in different genetic backgrounds with some idiosyncratic players, such as MAGEA5 (14).

Depletion of testis proteins disrupts bipolar spindle formation in the presence of paclitaxel. To determine if members of this testis cohort influence mitotic spindle architecture, we examined the distribution of γ-tubulin and pericentrin in mitotic cells depleted of these proteins and exposed to 10 nM paclitaxel. We found that disruption of each of these proteins led to an increase in the generation of spindles with more than 2 poles in the presence of 10 nM paclitaxel (Fig. 3A). In the case of MAGEA5 depletion, the majority of cells showed colocalization for pericentrin and γ-tubulin (Fig. 3B). This phenotype was similar to that with TACC3, which has been reported to contribute to centrosome clustering in tumor cells, suggesting that MAGEA5 may impact centrosomal duplication or coalescence (Fig. 3B) (13). On the other hand, FMR1NB-, NXF2-, STARD6-, and FSIP1-depleted cells contained multiple cytasters that were γ-tubulin positive but pericentrin negative (referred to herein as γ-tubulin bundles) (Fig. 3B). γ-Tubulin has been implicated in supporting *de novo* microtubule nucleation, as well as plus-end and lateral microtubule anchoring, thereby promoting acentrosomal microtubule nucleation during mitosis (22). Thus, these testis proteins may regulate microtubule nucleation and/or anchoring events in the mitotic spindle which are disrupted in the presence of paclitaxel.

NXF2, FSIP1, and STARD6 overexpression induces mitotic errors. Given the mitotic defects associated with depletion of this cohort of proteins, we evaluated the consequences of their overexpression in H1299 NSCLC cells. We have previously demonstrated that overexpression of ACRBP and FMR1NB can inhibit mitotic arrest induced by high levels of paclitaxel in H1155 cells (43, 46). A similar observation has also been reported for TACC3 (43, 46). In contrast, we found that overexpression of NXF2, FSIP1, and STARD6, in the absence of paclitaxel, increased the generation of multinucleated cells, a hallmark of aberrant mitosis (Fig. 4). The observation that mitotic defects are increased follow-

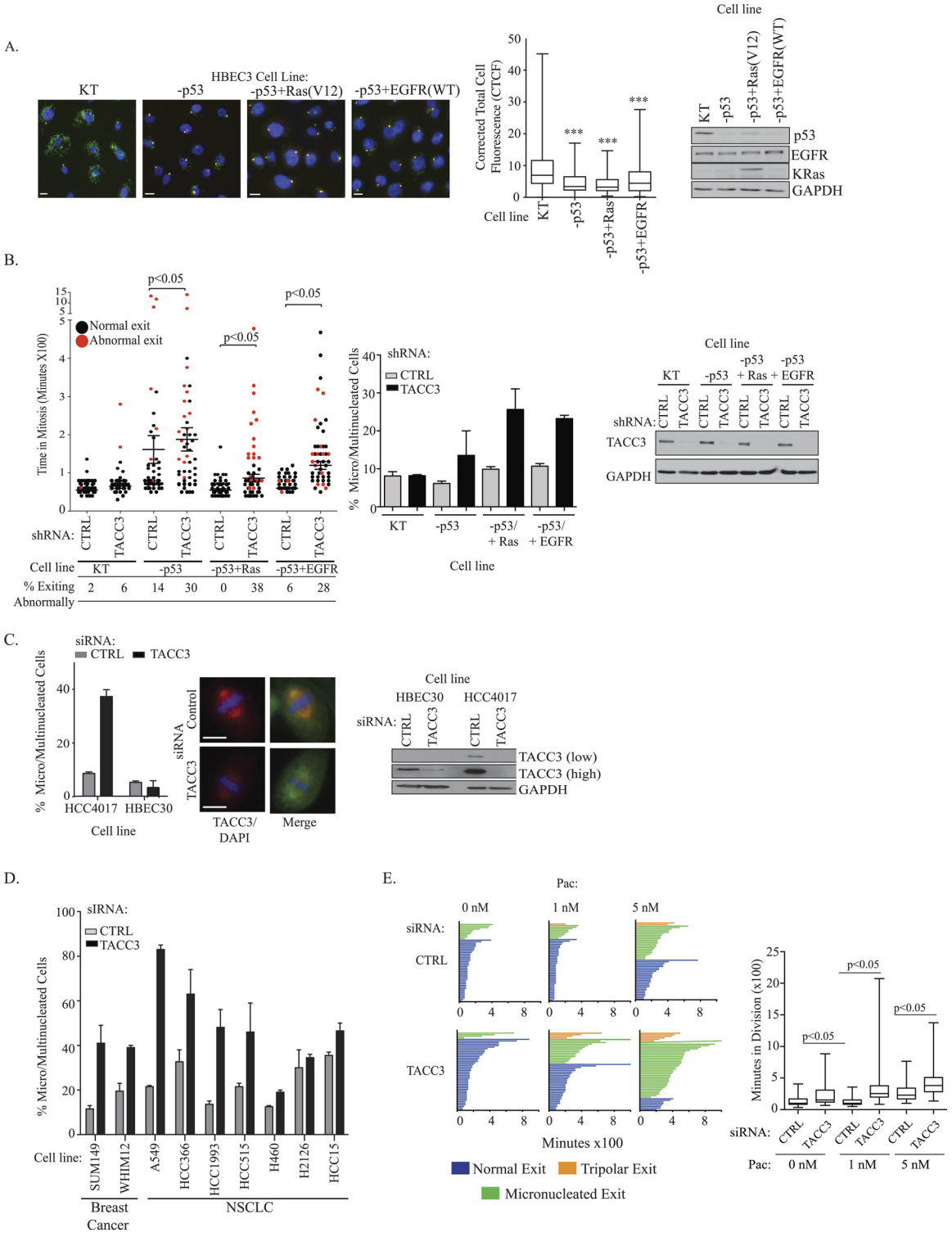

FIG 6 TACC3 is required for high-fidelity mitosis following oncogenic alterations. (A) HBEC3 cells with indicated stable genetic alterations were processed as for Fig. 5A. Left panels are representative images of immunostained cells. Middle panel is fluorescent quantitation of individual cells. *P* value was calculated by the Mann-Whitney *U* test. Scale bars are 10 μm. The right panel is an immunoblot of lysates from HBEC3KT series validating molecular changes. (B) The indicated HBEC3 cell lines expressing GFP-histone H2B were lentivirally infected with the indicated shRNAs. (Left) Five days postinfection, cells were plated and imaged by time-lapse microscopy for 48 h. Single-cell lineage tracing for each condition was performed to measure the outcome and length of mitosis as a function of the time from prometaphase to telophase in 50 cells. Quartile ranges for condition are shown. *P* values were calculated with the Mann-Whitney test. (Middle) At 7 days postinfection, cells were immunostained with antitubulin, antipericentrin, and DAPI. Results are averages of two experiments, with the error bars representing ranges. (Right) Immunoblot indicates TACC3 protein levels following stable knockdown. (C) The indicated cell lines were transfected with either a control or TACC3-targeting siRNAs. Forty-eight hours posttransfection, cells were exposed to 0.1 nM paclitaxel. (Left) Cells were fixed and stained with antibodies recognizing tubulin, pH3B, or TACC3 and DAPI. Multinucleated or micronucleated cells were scored by microscopic inspection. Error bars represent

ing either a decrease or increase in NXF2, FSIP1, or STARD6 protein levels suggests that they support dynamic processes which, when disturbed, lead to an aberrant mitosis. Indeed, commensurate phenotypes following gain or loss of function of Aurora-A and PLK1, key regulators of mitosis, have been reported (21, 25, 26, 28). A similar paradox has also been observed for MAD2, as either its overexpression or its haploinsufficiency increases tumor incidence in mice (27, 40). The effects of NXF2, FSIP1, and STARD6 may be indirect, as we did not observe a strong enrichment of these proteins at the centrosome or on microtubules. We did find that NXF2 was present in both the nuclear and cytoplasmic compartments, consistent with its putative role as an mRNA transport protein in sperm (Fig. 4) (26). We did not detect any significant defects following MAGEA5 overexpression, even in the presence of paclitaxel (data not shown).

Depletion of testis proteins alters microtubule sensitivity to nocodazole. Since proper microtubule dynamics are essential for a high-fidelity mitosis, we evaluated whether members of this cohort had any generalizable consequences on microtubule properties. To do this, we examined the microtubule network in target-depleted H1299 cells following a 30-min pulse with nocodazole. Under these conditions, a large portion of the microtubule network was depolymerized, while a small population of microtubules remained intact in control cells. However, RNA interference (RNAi) of FMR1NB, FSIP1, and TACC3 enhanced depolymerization, leaving few microtubules intact. Conversely, microtubules in STARD6-depleted cells were less sensitive to nocodazole (Fig. 5A). siRNA of NXF2 did not impact depolymerization properties but attenuated centrosomal regrowth at 2 min after nocodazole washout (Fig. 5B). We did not examine MAGEA5 in this study due to its lack of phenotype in mitotic assays in H1299 cells. The observed alterations in microtubule stability suggest that these proteins may be essential for proper microtubule function and could account for how they enhance paclitaxel sensitivity in tumor cells.

The dependency of polymer stability on these anomalously expressed proteins suggests that the microtubule network in tumor cells may have altered properties that require the participation of unique components compared to nontransformed cells. Indeed, alterations in the microtubule isotypes have been reported to occur frequently in breast cancer cells (28). Furthermore, mitotic microtubules in tumor cells display enhanced microtubule/kinetochore attachments compared to normal, immortalized counterparts (3, 32). To evaluate whether the stability of interphase microtubules is altered during tumor evolution, we assessed whether molecular changes that induce transformation may also lead to changes in microtubule dynamics. For this analysis, we examined microtubule stability in an isogenic cell line series of immortalized human bronchial epithelial cells (HBEC). This cell line series begins with an immortalized human bronchial epithelial cell line (HBEC3) that stably expresses CDK4 and hTERT (HBEC3KT). This parent line is then depleted of p53 alone or in combination with K-RAS or epidermal growth factor receptor (EGFR) overexpression (34). In this study, we exposed each of these different lines to high-dose nocodazole for 30 min and evaluated microtubule depolymerization properties. This analysis revealed that microtubules are more sensitive to nocodazole following loss of p53. This phenotype was not altered in the presence of overexpressed K-RAS or EGFR (Fig. 6A).

We next evaluated whether these isogenic cell lines are differentially sensitive to gametogenic gene disruption. We studied TACC3, as its expression is detectable in HBEC3KT cells. We examined whether stable TACC3 depletion altered mitotic progression in each of these cell lines by monitoring mitotic timing and outcome using live-cell imaging (Fig. 6B). This analysis was performed in the absence of paclitaxel. Depletion of TACC3 in strains with p53 deletion alone or in combination with RASV12 and EGFR enhanced both mitotic transit time and the frequency of abnormal exits, defined as either micro- or multinucleation (Fig. 6B). These abnormal products of mitosis could also be observed in fixed cells stably depleted of TACC3 (Fig. 6B). Furthermore, transient TACC3 depletion also enhanced the sensitivity of HCC4017 NSCLC cells to paclitaxel, but no significant impact was observed in an immortalized nonmalignant bronchial epithelial line, HBEC30, isolated from the same individual (Fig. 6C). We then evaluated the penetrance of the mitotic defects observed following TACC3 perturbation in a panel of lung- and breast tumor-derived cell lines. We found that TACC3 depletion, in the presence of low-dose paclitaxel, leads to an increase in mitotic abnormalities in 4 of the 7 NSCLC cells and the two triple-negative breast cancer (TNBC) cell lines we assayed (Fig. 6D). Additionally, TACC3 depletion prolonged mitotic transit time and increased abnormal segregation of chromosomes in ovarian cells isolated from patient ascites (Fig. 6E). Thus, at least in the case of TACC3, oncogenic changes can drive a dependency on TACC3 for high-fidelity mitosis in a range of genetic backgrounds, potentially due to underlying alterations in the microtubule network.

Gametogenic proteins may represent novel entry points for therapy. The restricted expression pattern of this cohort of gametogenic proteins and their requirement for deflecting mitotic perturbation suggest that they could represent unique entry points to enhance paclitaxel sensitivity in tumor cells. The recent discovery of a TACC3 inhibitor, KHS101, affords the opportunity to evaluate the therapeutic potential of targeting a reactivated gametogenic protein to enhance sensitivity to the first-line chemotherapeutic paclitaxel (44). To evaluate this possibility, we exposed H1155 cells to a combination of KHS101 and paclitaxel at doses with little or no single-agent activity. This combination led to enhanced cleaved caspase-3, unlike the use of either compound as a single agent (Fig. 7A). The combination also potently impacted mitosis and increased the accumulation of both mitotically ar-

average deviations for a minimum of 2 independent experiments. (Middle) Representative image of loss of HBEC30 cells transfected with siRNA targeting TACC3. HBEC30 cells are immunostained with antitubulin (green) and anti-TACC3 (red) and DAPI (blue). Scale bar is 10 μm. (Right) Immunoblot with the indicated antibodies and exposure levels of HBEC30 and HCC4017 lysates transfected with the indicated siRNAs for 72 h. (D) The indicated cell lines were transfected with either control or TACC3-targeting siRNA. Forty-eight hours posttransfection, cells were exposed to paclitaxel for 24 h with doses described in Materials and Methods. Cells were fixed and immunostained with antibodies recognizing pH3B, β-tubulin, and DAPI. Multi- or micronucleation was scored by microscopic inspection. Error bars represent deviations from the means for a minimum of 2 independent experiments. (E) (Left) Single-cell lineage tracing in LCOV2 cells for each condition was performed to measure the outcome and length of mitosis as a function of the time from prometaphase to telophase in 50 cells. (Right) Quartile ranges for mitotic transit time are shown. *P* values were calculated with the Mann-Whitney *U* test.

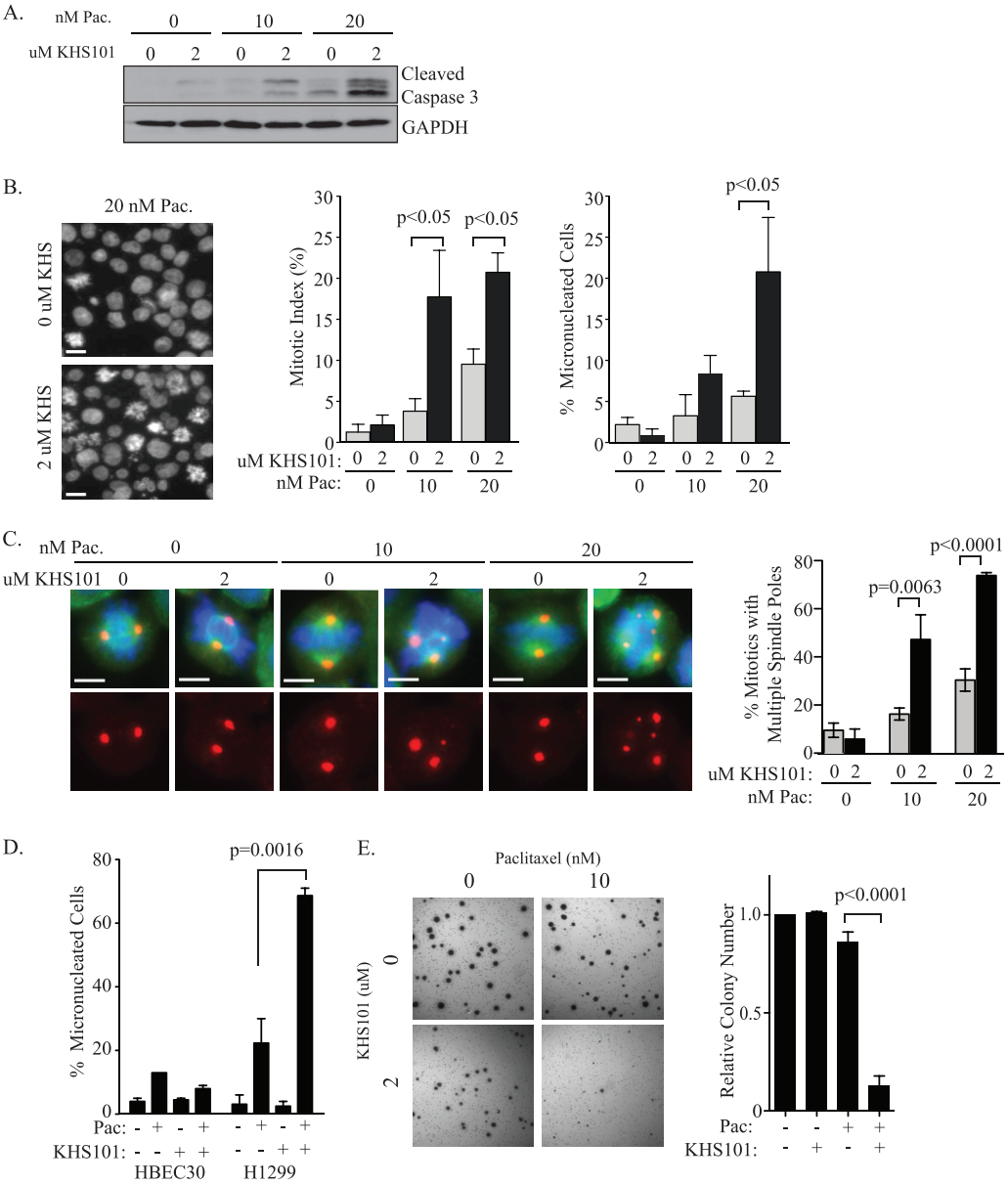

FIG 7 KHS enhances the effectiveness of paclitaxel. (A) H1155 cells were exposed to the indicated amounts of paclitaxel for 24 h, followed by incubation with the indicated KHS101 concentrations for 48 h. Whole-cell lysates were immunoblotted with the indicated antibodies. (B) H1155 cells were exposed to the indicated amounts of paclitaxel for 24 h, followed by incubation with the indicated KHS101 concentrations for 24 h, fixed, and immunostained with anti-pH3B, anti-β-tubulin, and DAPI. Cells were scored microscopically for mitosis and micronucleation (right). Error bars represent SEMs from 3 independent experiments. Student's *t* test was used to calculate *P* value. Scale bar is 10 μm. (C) H1155 cells were treated as for panel A, fixed, and immunostained with anti-β-tubulin (green), antipericentrin (red), and DAPI (blue). (Left) Representative images of cells treated as indicated. Scale bar is 5 μm. (Right) quantitation of abnormal spindles that were scored microscopically as any spindle having >2 centrosomes. Error bars represent SEMs from 3 independent experiments. Student's *t* test was used to calculate *P* value. (D) H1299 and HBEC30 cells were treated with 10 and 0.1 nM paclitaxel, respectively, and 2 μM KHS101 (as indicated) for 48 h and then fixed and immunostained with antitubulin, anti-pH3b, and DAPI. Micronucleated cells were scored by microscopic inspection. Error bars represent SEMs. Student's *t* test was used to calculate *P* value. (E) H1155 cells were seeded in soft agar and exposed to the indicated concentrations of paclitaxel and KHS101. Treatments were repeated every 5 days. Colonies were scored microscopically. Error bars represent SDs for three independent experiments.

rested and micronucleated cells (Fig. 7B). Examination of the mitotic spindle revealed numerous multipolar spindles with multiple, pericentrin-positive foci, a hallmark of TACC3 malfunction (Fig. 7C) (45). Suggesting that the combination may have efficacy in additional genetic backgrounds, cotreatment of H1299 cells with paclitaxel and KHS101 induced aberrant mitosis above levels detected for either agent alone (Fig. 7D). We did not observe defects in normal, immortalized HBEC30 cells cotreated with paclitaxel and KHS101 (Fig. 7D). In addition, anchorage-independent growth was diminished when H1155 cells were exposed to the KHS-paclitaxel combination compared to the use of either agent alone (Fig. 7E). Collectively,

these results reveal that the testis proteins frequently expressed in tumor can be essential for tumor cell fecundity and thus may present therapeutic entry points to enhance the efficacy of first-line chemotherapeutic agents.

DISCUSSION

Here, we describe a role for five testis proteins in supporting mitotic fidelity in cancer cells. We found that their disruption perturbs bipolar spindle assembly and chromosome segregation in the presence of paclitaxel. The altered sensitivity of microtubules to nocodazole following depletion of these proteins suggests that the observed synergy with paclitaxel could result from a convergence on microtubule stability. Importantly, these proteins appear to normally have a testis-biased expression pattern, and in particular, the CT antigens NXF2, FMR1NB, and MAGEA5 are highly testis restricted and not detectable in normal somatic tissues. In addition to our findings here, we have previously reported a mitotic role for the CT antigen ACRBP in cancer cells (43). The roles of these CT antigens in spermatogenesis are unclear; however, they could represent a coordinated network that, when reactivated in tumor cells, supports mitosis. Thus, our collective findings indicate that reactivated testis proteins are not simply epiphenomena but may be engaged to support tumor cell division and fecundity. Importantly, the demonstration that inhibition of TACC3, a tumor-activated testis protein, can enhance the effects of paclitaxel in tumor, but not normal, cells indicates the potential of reactivated testis proteins as therapeutic entry points.

Well-established mitotic proteins, TACC3 and MAD2, share the stress-induced defects we observed following depletion of this cohort. The similarity in phenotypes indicates a role for these testis proteins in supporting mitotic resilience. This finding suggests that tumor cells may maintain a molecular buffer that allows for the deflection of environmental insults during cell division. This mitotic robustness may emerge during tumor evolution to overcome barriers inhibiting accurate chromosome segregation. For example, our findings that microtubule stability is altered following p53 deletion indicate that tumor suppressor loss, while restraining cell suicide programs, may have collateral impacts on the cytoskeleton. Thus, population variants that are able to circumvent this barrier to outgrowth would have a selective advantage. Anomalous gene expression programs activated during tumorigenesis may provide a supply of otherwise unavailable proteins for overcoming growth inhibition, and we postulate that reactivated testis proteins may be engaged for this purpose.

Based on our findings here, future molecular analysis will decode the mechanisms by which these components serve to directly or indirectly support mitosis. While minimal information exists on their role in spermatogenesis, some potential inferences based on implied roles can be postulated. For example, NXF2 knockout mice undergo meiotic defects, suggesting that the meiotic role of NXF2 is hijacked in transformed cells. In particular, NXF2 has been implicated as an mRNA nuclear transport protein similar to RAE1, which can alter the microtubule cross-linking activity of NUMA and impede bipolar spindle formation. Other members of this cohort have nonmitotic roles in spermatogenesis, suggesting that they are neomorphically engaged by the tumor cell mitotic network. For example, FSIP1 is a component of the microtubule- and dynein-rich fibrous sheath structure, which is essential for flagellum function and sperm movement. Expression levels of FSIP1 are elevated in breast cancer, suggesting that its activation is frequent and may be important functionally (30; see also https://www.oncomine.org/resource/login.html). Given that tumor cells lack flagella, FSIP's microtubule and dynein regulatory properties may be anomalously engaged to support the microtubule network and reinforce mitotic robustness in tumor cells. Furthermore, FSIP1 interacts with a number of additional proteins in the fibrous sheath, AKAP3, AKAP4, ROPN1, SPA17, and CABYR, which are all classified as CT antigens (5, 11, 17). ODF2 and SPAG5 are also fibrous sheath proteins that are required for centrosome and kinetochore function in tumor cells (16, 18, 23, 24, 38). Thus, the elements that regulate the microtubule-rich fibrous sheath structure could be coordinately reactivated in tumor cells, as they may confer mitotic robustness. Revealing the proximal mechanistic connections of these testis proteins to mitotic spindle function has great potential for uncovering differences between mitosis in tumor and normal cells. Concomitantly, this mechanistic elaboration may also identify additional therapeutic entry points to enhance the tumoricidal activity of paclitaxel or other first-line microtubule-disrupting agents.

ACKNOWLEDGMENTS

This work was supported by Public Health Service grants CA154699 and CA128926 to A.W.W. from the National Cancer Institute and an Innovative Research Grant from Stand Up to Cancer. K.M.C. and P.T. are supported by general medicine training grant GM008719 and the NCI training grant CA071341-14 (K.M.C.). K.M. and R.S. were supported by general medicine training grant T32GM007040-37.

We thank Peter Schultz for providing KHS101. We thank John Minna and Jill Larsen for HBEC3 cells.

REFERENCES

1. **Abell AN, et al.** 2011. MAP3K4/CBP-regulated H2B acetylation controls epithelial-mesenchymal transition in trophoblast stem cells. Cell Stem Cell **8**:525–537.
2. **Aitola M, Sadek CM, Gustafsson JA, Pelto-Huikko M.** 2003. Aint/Tacc3 is highly expressed in proliferating mouse tissues during development, spermatogenesis, and oogenesis. J. Histochem. Cytochem. **51**:455–469.
3. **Bakhoum SF, Genovese G, Compton DA.** 2009. Deviant kinetochore microtubule dynamics underlie chromosomal instability. Curr. Biol. **19**: 1937–1942.
4. **Bose HS, et al.** 2008. StAR-like activity and molten globule behavior of StARD6, a male germ-line protein. Biochemistry **47**:2277–2288.
5. **Brown PR, Miki K, Harper DB, Eddy EM.** 2003. A-kinase anchoring protein 4 binding proteins in the fibrous sheath of the sperm flagellum. Biol. Reprod. **68**:2241–2248.
6. **Buffin E, Emre D, Karess RE.** 2007. Flies without a spindle checkpoint. Nat. Cell Biol. **9**:565–572.
7. **Cappell KM, Larson B, Sciaky N, Whitehurst AW.** 2010. Symplekin specifies mitotic fidelity by supporting microtubule dynamics. Mol. Cell. Biol. **30**:5135–5144.
8. **Caron C, et al.** 2010. Functional characterization of ATAD2 as a new cancer/testis factor and a predictor of poor prognosis in breast and lung cancers. Oncogene **29**:5171–5181.
9. **Conte N, et al.** 2003. TACC1-chTOG-Aurora A protein complex in breast cancer. Oncogene **22**:8102–8116.
10. **Doyle JM, Gao J, Wang J, Yang M, Potts PR.** MAGE-RING protein complexes comprise a family of E3 ubiquitin ligases. Mol. Cell **39**:963–974.
11. **Eddy EM, Toshimori K, O'Brien DA.** 2003. Fibrous sheath of mammalian spermatozoa. Microsc. Res. Tech. **61**:103–115.
12. **Epping MT, et al.** 2005. The human tumor antigen PRAME is a dominant repressor of retinoic acid receptor signaling. Cell **122**:835–847.
13. **Fielding AB, Lim S, Montgomery K, Dobreva I, Dedhar S.** 2011. A critical role of integrin-linked kinase, ch-TOG and TACC3 in centrosome clustering in cancer cells. Oncogene **30**:521–534.
14. **Gascoigne KE, Taylor SS.** 2008. Cancer cells display profound intra- and

interline variation following prolonged exposure to antimitotic drugs. Cancer Cell **14**:111–122.

14a. **Gazdar AF, Oie HK.** 1986. Correspondence re: Martin Brower et al. Growth of cell lines and clinical specimens of human non-small cell lung cancer in a serum-free defined medium. Cancer Res., **46**:798–806, 1986. Cancer Res. 46:6011–6012. (Letter.)

15. **Gergely F, Draviam VM, Raff JW.** 2003. The ch-TOG/XMAP215 protein is essential for spindle pole organization in human somatic cells. Genes Dev. **17**:336–341.

16. **Gruber J, Harborth J, Schnabel J, Weber K, Hatzfeld M.** 2002. The mitotic-spindle-associated protein astrin is essential for progression through mitosis. J. Cell Sci. **115**:4053–4059.

17. **Hofmann O, et al.** 2008. Genome-wide analysis of cancer/testis gene expression. Proc. Natl. Acad. Sci. U. S. A. **105**:20422–20427.

18. **Ibi M, et al.** 2011. Trichoplein controls microtubule anchoring at the centrosome by binding to Odf2 and ninein. J. Cell Sci. **124**:857–864.

19. **Jung CK, et al.** 2006. Expression of transforming acidic coiled-coil containing protein 3 is a novel independent prognostic marker in non-small cell lung cancer. Pathol. Int. **56**:503–509.

20. **Lai D, Sakkas D, Huang Y.** 2006. The fragile X mental retardation protein interacts with a distinct mRNA nuclear export factor NXF2. RNA **12**: 1446–1449.

21. **Liu X, Lei M, Erikson RL.** 2006. Normal cells, but not cancer cells, survive severe Plk1 depletion. Mol. Cell. Biol. **26**:2093–2108.

22. **Lüders J, Stearns T.** 2007. Microtubule-organizing centres: a re-evaluation. Nat. Rev. Mol. Cell Biol. **8**:161–167.

23. **Mack GJ, Compton DA.** 2001. Analysis of mitotic microtubule-associated proteins using mass spectrometry identifies astrin, a spindle-associated protein. Proc. Natl. Acad. Sci. U. S. A. **98**:14434–14439.

24. **Manning AL, et al.** 2010. CLASP1, astrin and Kif2b form a molecular switch that regulates kinetochore-microtubule dynamics to promote mitotic progression and fidelity. EMBO J. **29**:3531–3543.

25. **Marumoto T, et al.** 2003. Aurora-A kinase maintains the fidelity of early and late mitotic events in HeLa cells. J. Biol. Chem. **278**:51786–51795.

26. **Meraldi P, Honda R, Nigg EA.** 2002. Aurora-A overexpression reveals tetraploidization as a major route to centrosome amplification in p53−/− cells. EMBO J. **21**:483–492.

27. **Michel LS, et al.** 2001. MAD2 haplo-insufficiency causes premature anaphase and chromosome instability in mammalian cells. Nature **409**:355–359.

28. **Mundt KE, Golsteyn RM, Lane HA, Nigg EA.** 1997. On the regulation and function of human polo-like kinase 1 (PLK1): effects of overexpression on cell cycle progression. Biochem. Biophys. Res. Commun. **239**:377–385.

29. **Pan J, et al.** 2009. Inactivation of Nxf2 causes defects in male meiosis and age-dependent depletion of spermatogonia. Dev. Biol. **330**:167–174.

30. **Radvanyi L, et al.** 2005. The gene associated with trichorhinophalangeal syndrome in humans is overexpressed in breast cancer. Proc. Natl. Acad. Sci. U. S. A. **102**:11005–11010.

31. **Ramirez RD, et al.** 2004. Immortalization of human bronchial epithelial cells in the absence of viral oncoproteins. Cancer Res. **64**:9027–9034.

32. **Rao S, Aberg F, Nieves E, Band Horwitz S, Orr GA.** 2001. Identification by mass spectrometry of a new alpha-tubulin isotype expressed in human breast and lung carcinoma cell lines. Biochemistry **40**:2096–2103.

33. **Sadek CM, et al.** 2003. TACC3 expression is tightly regulated during early differentiation. Gene Expr. Patterns **3**:203–211.

34. **Sato M, et al.** 2006. Multiple oncogenic changes (K-RAS(V12), p53 knockdown, mutant EGFRs, p16 bypass, telomerase) are not sufficient to confer a full malignant phenotype on human bronchial epithelial cells. Cancer Res. **66**:2116–2128.

35. **Schmidt S, et al.** 2010. The centrosomal protein TACC3 controls paclitaxel sensitivity by modulating a premature senescence program. Oncogene **29**:6184–6192.

36. **Schneider L, et al.** 2008. TACC3 depletion sensitizes to paclitaxel-induced cell death and overrides p21WAF-mediated cell cycle arrest. Oncogene **27**:116–125.

37. **Schneider L, et al.** 2007. The transforming acidic coiled coil 3 protein is essential for spindle-dependent chromosome alignment and mitotic survival. J. Biol. Chem. **282**:29273–29283.

38. **Shao X, Xue J, van der Hoorn FA.** 2001. Testicular protein Spag5 has similarity to mitotic spindle protein Deepest and binds outer dense fiber protein Odf1. Mol. Reprod. Dev. **59**:410–416.

39. **Simpson A, Caballero OL, Jungbluth A, Chen YT, Old LJ.** 2005. Cancer/testis antigens, gametogenesis and cancer. Nat. Rev. Cancer **5**:615–625.

40. **Sotillo R, et al.** 2007. Mad2 overexpression promotes aneuploidy and tumorigenesis in mice. Cancer Cell **11**:9–23.

41. **Takano K, Miki T, Katahira J, Yoneda Y.** 2007. NXF2 is involved in cytoplasmic mRNA dynamics through interactions with motor proteins. Nucleic Acids Res. **35**:2513–2521.

42. **Whitehurst AW, et al.** 2007. Synthetic lethal screen identification of chemosensitizer loci in cancer cells. Nature **446**:815–819.

43. **Whitehurst AW, et al.** 2010. Tumor antigen acrosin binding protein normalizes mitotic spindle function to promote cancer cell proliferation. Cancer Res. **70**:7652–7661.

44. **Wurdak H, et al.** 2010. A small molecule accelerates neuronal differentiation in the adult rat. Proc. Natl. Acad. Sci. U. S. A. **107**:16542–16547.

45. **Yao R, et al.** 2012. Disruption of Tacc3 function leads to in vivo tumor regression. Oncogene **31**:135–148.

46. **Yim EK, et al.** 2009. Anticancer effects on TACC3 by treatment of paclitaxel in HPV-18 positive cervical carcinoma cells. Oncol. Rep. **21**:549–557.